Scanning Microscopy

Volume 1992
Number 6 *Signal and Image Processing in Microscopy and Microanalysis*

Article 4

1992

Three-Dimensional Crystallographic Reconstruction for Atomic Resolution

Kenneth H. Downing
Lawrence Berkeley Laboratory, California

Scanning Microscopy Supplement 6, 1992 (pages 43-52) 0892-953X/92$5.00+.00
Scanning Microscopy International, Chicago (AMF O'Hare), IL 60666 USA

THREE-DIMENSIONAL CRYSTALLOGRAPHIC RECONSTRUCTION FOR ATOMIC RESOLUTION

Kenneth H. Downing

Donner Laboratory, Lawrence Berkeley Laboratory, Berkeley, CA 94720
Telephone No. (510) 486-5941 / FAX 485-5342

ABSTRACT

Three-dimensional structures have recently been determined by electron crystallography at a resolution high enough to determine atomic arrangements in both protein and mineral specimens. The different nature of these two types of specimens produces some very significant differences in the way data is obtained and processed, although the principles are the same. The sensitivity of proteins to damage by the electron beam limits the signal-to-noise ratio in the image and the resolution to which data can be extracted from the image. A number of constraints, such as the amino acid sequence and the connectivity of atoms within amino acids, can be used in interpreting the limited image data. In materials samples, the relative insensitivity to damage allows obtaining resolution limited only by the microscope. In many samples, dynamical scattering and other non-linear effects limit the information in the image, but this limit can be circumvented by working in very thin areas of the specimen.

Key Words: Electron crystallography, three-dimensional reconstruction, structure determination

Introduction

Images obtained in the electron microscope are necessarily views of the projection of the specimen. Each point in the image represents the sum of information in a column of the specimen along the beam direction. For many cases this projection image provides sufficient information to reveal the desired information about the specimen. However, as the level of detail and complexity in the image of a three-dimensional (3-D) structure increases, the interpretability of the image decreases, because more details of interest overlap in the projection. Combining images from different views of the specimen can provide the 3-D information that is necessary to resolve these overlaps and thus make the image interpretable.

Several approaches to obtaining 3-D information have been developed, ranging from simple stereo pairs to analysis of randomly oriented single molecules. Crystallographic approaches are presently among the most highly developed in terms of obtained resolution. The development of electron crystallography (Glaeser, 1985) has been driven mainly by biologists, who have both a need to resolve highly complicated structures and an opportunity to obtain useful structural information at the moderate resolution levels that have been within reach for many years. For example, structural domains within proteins can be resolved at the resolution provided by negative stains, around 2 nm (Amos et al. 1982). Helical reconstruction techniques were first developed, followed by reconstructions from tilt series, and applied to a wide variety of stained specimens.

Achieving a resolution high enough to determine atomic structures has long been a goal of electron crystallographers, but a number of technical problems had to be overcome in order to make the leap from 2 nm to atomic resolution. Among the first major advances was replacing the stain by a more appropriate embedment such as glucose (Unwin and Henderson, 1975) or vitreous ice (Dubochet et al. 1988). By retaining the native hydrated state of the specimen, these embedding materials preserved the

structure to high resolution, but introduced problems of low contrast and high susceptibility to radiation damage. These problems were in turn overcome by low dose imaging of cold specimens and extensive computer image processing (Henderson et al. 1986).

The first atomic model of a protein structure determined by electron crystallography was finally published in 1990 (Henderson et al. 1990). Bacteriorhodopsin (bR), a protein found in the membrane of the bacterium *Halobacterium halobium*, is extracted in two-dimensional sheets (purple membrane, PM) within which the protein is arranged on a crystalline lattice. Much of electron crystallography has developed around studies of purple membrane, and the methodology is now in place for rapid progress in applications to other protein structures. We will discuss this work as an example of applications in structural biology.

Applications of 3-D reconstruction in materials science have lagged behind biological work, for reasons entirely different from those which have limited biological applications, and in spite of the potential for significantly higher resolution. Among these reasons is the experience that images of materials samples are often affected by dynamical effects to such an extent that image interpretation required a comparison between the experimental images and computer simulations of images based on a proposed structural model (O'Keefe et al. 1978). Indeed, many of the important questions addressed by microscopists in materials science can be addressed by imaging specimens in projection, with appropriate image interpretation. Again, though, as image resolution improves, the overlap of individual atom images in a 3-D structure becomes a limit to the usefulness of projection images, and there is a great deal to gain by 3-D reconstruction.

We have recently expanded techniques used in biological electron crystallography to 3-D reconstruction with high-resolution images of a mineral, staurolite, and have obtained a reconstruction in which the atoms are clearly resolved (Downing et al. 1990). Through-focus series images from five different orientations of the sample were combined to derive the 3-D map. Although this work was undertaken with a specimen of known structure in order to demonstrate the methodology, application to unknown structures appears to be straightforward.

We will review requirements for obtaining data with protein and materials samples, and then discuss the actual crystallographic 3-D reconstruction process and interpretation of results, with particular attention to the differences between the two types of samples.

Electron Crystallography

Images as Projections of the 3-D Structure

A 3-D object can be represented by the full 3-D Fourier transform of the object. Figure 1 represents the arrangement of data in the transform of the limiting cases of thin and thick specimens. The Fourier transform of a projection of the object gives a central section of the 3-D Fourier transform - i.e., the values in the transform lying on a plane which passes through the origin. The essence of crystallography lies in sampling the 3-D transform at a sufficiently large number of points that the 3-D object structure can be reconstructed by inverse Fourier transformation. By recording images of the specimen at various tilt angles or orientations, different planes of the 3-D transform are sampled. Data from the various orientations are combined in the computer to fill Fourier (or reciprocal) space.

Within certain approximations the image in an electron microscope can be taken as a representation of the projection of the specimen. In most 3-D reconstruction schemes, these approximations must be valid, since to date the mathematics for treating the images has been developed only for this case. Deviations from this approximation can be attributed basically to the finite wavelength or energy of the electrons, and have been extensively investigated for many types of specimens. The finite wavelength, which corresponds to the curvature of the Ewald sphere, causes a deviation between the actual point of reciprocal space

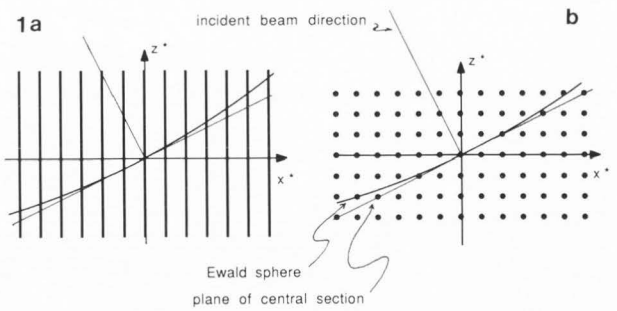

Fig. 1. Diagrams of reciprocal space corresponding to (a) a 2-D (monolayer) crystal, and (b) a 3-D crystal. The Ewald sphere is shown for an incident beam that is tilted away from the normal (corresponding to tilting the specimen). Amplitude and phase vary smoothly along lattice rods in (a), and the Ewald sphere intersects all rods, producing diffraction for all H,K indices, for any orientation of the specimen. Ideally the sphere would intersect the rods in a plane, but the finite curvature of the sphere causes deviations from the plane which become more significant at higher resolution and higher tilt. The discrete sampling of the reciprocal lattice of the 3-D crystal requires accurate orientation of the specimen in order to obtain diffraction at a large number of lattice points, and Ewald sphere curvature causes the lattice points to be missed at higher resolution. As the accelerating voltage increases, the sphere becomes flatter, more closely approximating the ideal plane.

sampled in the image and the ideal central plane. In biological samples, this becomes significant especially for highly tilted samples where symmetrically diffracted beams sample points that are assumed to be related by symmetry but in fact are not. In the case of 3-D crystals, the Ewald sphere curvature may cause diffraction spots to be missed or to show up at a specimen tilt angle different from that expected from the projection approximation (see Fig. 1).

The projection approximation generally assumes that the scattering of electrons by the specimen is weak. Dynamical scattering and other non-linear effects, which result from stronger scattering, can cause errors in the projection approximation. Problems arising from Ewald sphere curvature, dynamical scattering and non-linear effects are all reduced as the electron energy is increased, and the trend in high resolution work is clearly in the direction of microscopes operating at accelerating voltages higher than 100 kV.

Deviations from the projection approximation increase with increasing specimen thickness. For most organic specimens, the approximation is expected to hold for specimens thinner than about 25 nm, at 100 kV (Ho et al. 1988), while for inorganic specimens there may be significant deviations at thicknesses well below 5 nm (Hirsch et al. 1965). Most of the biological specimens of interest for high resolution work at present are on the order of 5 nm thick, about the size of moderate-sized proteins, and are thus well within the limit for the projection approximation. On the other hand, it is often difficult to obtain areas in materials samples that are uniformly thin over large enough areas for crystallographic imaging. With ion-beam thinned specimens, there is generally a wedge of at least 15° near the thinnest areas, so that areas less than 5 nm in thickness can be no more than 15 nm wide. We were able to work with these small areas, though, owing to the high signal-to-noise ratio (SNR) that can be obtained in the image.

Image Recording

The sensitivity of organic specimens to radiation damage by the electron beam requires that low-dose techniques be used for recording high-resolution images. In principle, the only significant electron exposure the specimen may receive is the exposure for recording the image. The image exposure itself is calculated to provide the best signal-to-noise ratio (SNR), and does cause serious damage to the specimen. Thus only a single image can be recorded of each crystalline area. For proteins cooled to -120C and exposed to 100 kV electrons, the exposure is about 1000 e/nm^2. For photographic films of moderate speed (e.g., Kodak SO-163 with fast developing conditions) this exposure will produce a reasonable darkening of the emulsion at a magnification of 50-60,000x. The low exposure on the photographic film essentially precludes use of much higher magnification, which is usually used for very high resolution work on more stable specimens. However, we have found that the modulation transfer function of the film is adequate for resolving the smallest details (Downing and Grano, 1982), and indeed the optimum magnification for this level of specimen exposure is in the 50,000x range.

This low exposure requires that searching for good specimen areas must be done at extremely low dose rates, and the image must be focused on an area adjacent to the area of interest. We have found that exposure rates of around 100 e/nm^2-min are adequate for clearly identifying good areas in many types of specimens when the image is viewed at a very low magnification with high defocus. A defocused diffraction mode is convenient for searching. Most modern microscopes are equipped with facilities for switching easily between modes for searching, focusing, and imaging. We have found it convenient to control microscope operation with an external computer for more flexibility than many microscopes offer, both with older, analog-electronics microscopes and with newer microscopes that have internal microprocessors.

Even with the best technique and equipment, the image is still very limited in SNR by the low exposure. There should be, for example, no expectation of resolving small details directly in the image of a protein molecule. One can estimate from the Rose equation (Rose, 1973) that the smallest detail with 10% contrast that could be seen in the image would be about 1.5 nm in size, and at high resolution, we are looking for details with much less contrast. The beauty of the crystallographic approach is that all of the information which is spread out with low SNR in the full image is concentrated, in the Fourier transform of the image, into a relatively small number of diffraction spots, which can be detected with a much better SNR than in the image. Extracting the data at these reciprocal lattice points and then reconstructing the image is mathematically equivalent to averaging all of the images of the unit cell in the crystal image. Considering that the SNR in a shot-noise limited image should increase with the square root of the number of unit cells that are averaged, we can estimate that high-resolution details should begin to emerge as we combine 10,000 to 100,000 unit-cell images.

The radiation resistance of many materials samples is in stark contrast to the sensitivity of organic specimens. Although the lifetime of most specimens in the beam is not unlimited, there is generally little difficulty in recording images that are statistically well defined even at high resolution. In this case, the magnification for photographic recording must be high enough to avoid

saturating the emulsion. In addition, it is possible both to focus carefully on the area of interest and to record focus series of images. In the staurolite work, focus series of up to ten images covering a defocus range of 120 nm were recorded.

The ability to examine the specimen extensively prior to image recording is especially important in adjusting the orientation along principal zone axes. Although the specimens are thin, they will still generally be several unit cells thick, and the reciprocal lattice will consist of spots which are sharp in all directions. Careful alignment of orientation, so that many reflections are excited simultaneously, becomes critical.

Many, although not all, of the biological specimens which have been investigated by electron crystallography are true monolayer or two-dimensional crystals - i.e., a single unit cell thick. In this case, the reciprocal lattice consists of lattice rods, rather than spots, running in the direction perpendicular to the specimen plane (see Fig. 1). One can thus afford to be quite imprecise in orienting the sample, since reflections on every lattice rod will be present for any specimen orientation. In fact, one generally collects images with specimen tilt or azimuth angles distributed as uniformly as possible up to the maximum available tilt in order to sample all of the lattice rods with some redundancy.

The range of tilt angles available is set by several factors related to having the thin, plate-like specimen on a support film. As the tilt angle is increased much above 60°, the projected specimen thickness rapidly becomes prohibitively large and the available specimen area becomes too small. Although some applications have used tilt angles even higher than 80° (Baumeister et al. 1986), the 60° limit has been generally adopted, and is often the limit of goniometer tilt. The resulting "hollow cone" of reciprocal space within which data is not obtained can introduce artifacts in image reconstructions at low resolution, although it has been shown recently that this is not a problem at high resolution (Glaeser et al. 1989).

The hollow cone problem does not necessarily arise in materials samples, where specimens can be cut from the bulk in any desired orientation. In our work on staurolite, for example, we used three sections cut along the three orthogonal axes. The problem in obtaining data to fill reciprocal space in this case is more in finding orientations in which there is a high density of diffraction spots. With images from five orientations of staurolite, and the crystallographic symmetry of the sample, we were able to sample the entire 3-D reciprocal space sufficiently to obtain nearly isotropic resolution.

Image Processing

The steps of image processing lead up to extraction of structure factors from the Fourier transform of the image. Again, differences in the nature of images of biological and materials samples necessitate differences in the data handling. Images are first scanned on a densitometer to read the data into the computer. The spacing between sampling points is determined by the resolution anticipated from the image. Protein images are sampled with a step size corresponding to around 0.15 nm at the specimen, or about 10 μm on the film, while mineral images have been sampled at 0.05 nm (25 μm). Images of unstained protein crystals are generally sampled on an array of at least 1000x1000, and often up to 6000x6000, image elements (pixels), in order to include enough unit cells to obtain a good SNR at high resolution. The size of the array is limited to some extent both by the crystal size and the capacity of the computer. One would like to include as much image area as possible in the scan, but finite disk space for storing the scan and the many files created during processing have set a practical limit presently at about 6000x6000 pixels (the transform of such an array contains 144 Mbytes!). We can look forward to being able to increase the array size with larger computers, and expect that high-resolution information should become even easier to extract from the images. Few proteins have so far been crystallized in arrays large enough to justify this large a scan array, however, and the scan size for smaller crystalline arrays is adjusted to fit the crystal. The high SNR in images of minerals allows us to use much smaller image areas, and indeed, the limited area within which the specimen is thin enough for the projection approximation to apply sets an upper limit to the area which can be treated. We used arrays of 400x400 pixels throughout the work with staurolite.

After the Fourier transform is calculated, it is displayed for interactive indexing. Examples of computed transforms are shown in Fig. 2. Miller indices, H,K, are assigned to each reciprocal lattice point by identifying positions of a few spots, and fitting a lattice to the points. For two-dimensional crystals at any tilt angle, these indices will generally correspond to the indices of the lattice rods, i.e., to the corresponding lattice points in the transform of the untilted image. In the case of 3-D crystals, the H,K indices will have to be transformed later to the 3-D hkl indices of the full 3-D reciprocal space. The transformation should be clear since the corresponding electron diffraction pattern is indexed during the process of orienting the crystal in the microscope.

Two-dimensional arrays of biological molecules are not very rigid, and it is observed that some distortions are present in the images. Especially when very large image areas are processed, it is necessary to correct for these distortions, or else the diffraction spots will be spread over several pixels of the transform and thus will tend to be lost in the noise. Procedures for

this distortion correction, based on correlation of the full image with the image of a small number of unit cells, have been used with great success (Henderson et al. 1986). The mineral samples, on the other hand, are quite rigid, and over the very small areas processed, no distortions or defects were observed. On the contrary, the diffraction spots were so strong and well defined that the expected tails of the spots could be followed in the transform for long distances from the center of the spots, as seen in Fig. 2b.

Contrast Transfer Function

After the data at the reciprocal lattice points is extracted from the Fourier transform, effects of the contrast transfer function of the microscope must be dealt with. Effects of defocus are familiar in the Thon rings seen in transforms of amorphous specimens. The exposure in images of proteins is often not sufficient for the contribution of the amorphous component to be seen clearly, but the density of diffraction spots in the transform is high enough that the rings show up in the transform of the protein crystal itself (see Fig. 2a). The variation of diffraction spot intensity in the transform can then be used to determine defocus parameters which are then used to correct the sign of the structure factors.

The unit cell of materials samples is often so small that not enough spots are present in the transform to identify zeros of the CTF (see Fig. 2b). The zeros do show up for the amorphous component, but extend only to around 0.2-0.3 nm with enough contrast to be helpful in determining the CTF. More accurate determination of defocus is necessary for utilization of information at higher resolution, where the sign of the CTF can vary rapidly with small changes in defocus. We have again used the variation of diffraction spot amplitude, in this case within the defocus series, to determine defocus values. Some examples are shown in Fig. 3, where the amplitudes of each reflection for all members of a focus series are plotted as a function of defocus. An iterative process was developed that varies the presumed starting defocus of the focus series and searches for the best consistency of resultant phases from all images throughout the series. In Fig. 3 the resultant CTF (as a function of defocus) is plotted along with the amplitudes. This procedure is limited by the sensitivity of the amplitudes to dynamical effects, and indeed the fit is far from perfect in this example. However, the consensus phase values appear quite reliable, and the procedure allowed extraction of accurate phases to a resolution well beyond any direct indication of zeros in the CTF.

In any case, it is necessary to use images taken at more than one defocus to fill in data near the zeros of the CTF in a single image.

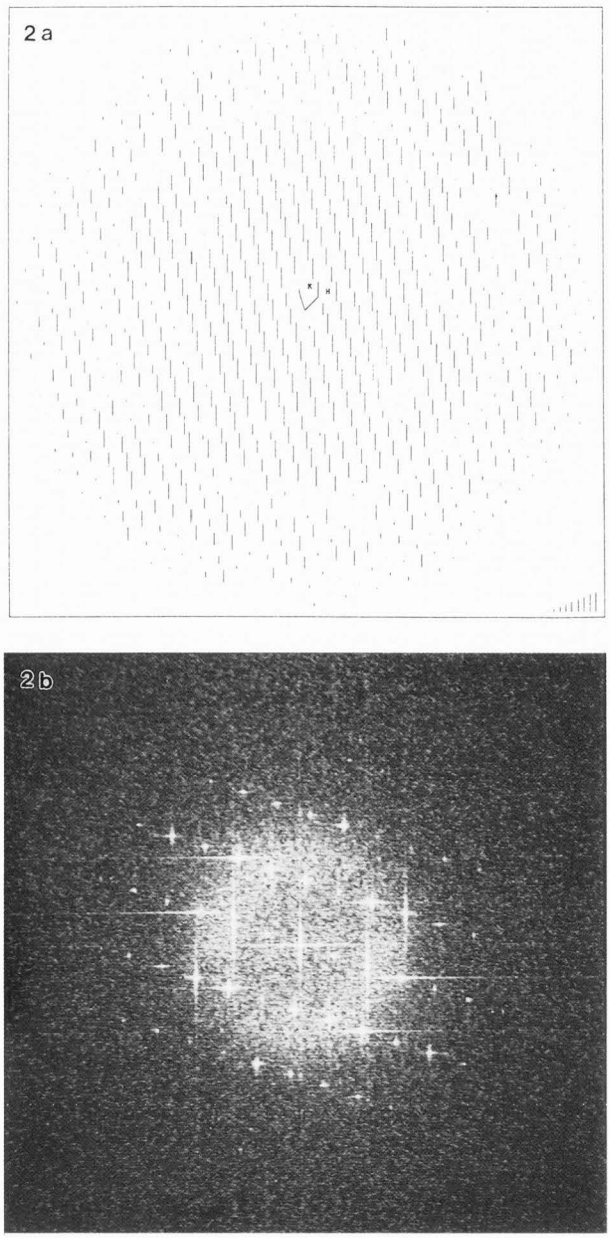

Fig. 2. Computed Fourier transforms of (a) untilted bR, (b) staurolite in [101] orientation. The diagram in (a) represents the SNR found at each reciprocal lattice point of the specimen; zeros of the contrast transfer function are clear in rings where the SNR is low, at about the 7th and 11th orders. The edge of the plot corresponds to 0.35 nm. In (b), the figure extends to 0.1 nm, and diffraction spots are present to at least 0.14 nm. The variation of the CTF shows up clearly from the amorphous component of the specimen, but extends only to around 0.2 nm. This image was recorded at 800 kV with a defocus of about 110 nm, about two times the Scherzer defocus.

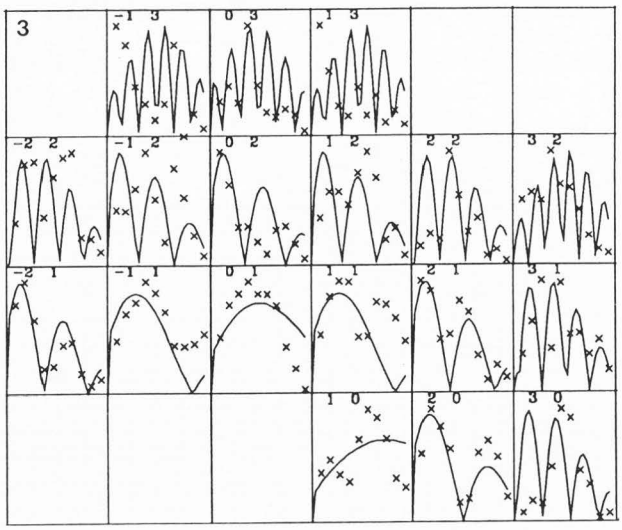

Fig. 3. Variation in diffraction amplitudes found in transforms of a through-focus image series. Plots are shown for each reflection, with defocus on the horizontal axis. The absolute value of the CTF is indicated by the smooth curves. For each reflection, the plot is scaled to the maximum amplitude found in the focus series. Images were recorded at 800 kV with focus steps of 12 nm.

Structure Factor Amplitudes

It has long been recognized that amplitudes of structure factors derived from image data are much less reliable than those determined from electron diffraction patterns, when the electron diffraction can in fact be obtained. Image amplitudes are subject to effects such as variation of the CTF and beam-induced specimen motion, which can not always be precisely compensated. Electron diffraction patterns from purple membrane, for example, can be obtained from areas about 10 times as large as areas used in images, allowing lower electron exposure and thus less damage during recording, and highly accurate measurement of spot amplitudes. Figure 4a shows an example of the amplitudes extracted from an image relative to those determined from diffraction. There is a strong loss of signal in the image at high resolution that results from a combination of several factors (Henderson and Glaeser, 1985). In reconstructing an image, it is then preferable to use amplitudes derived from electron diffraction, and phases determined from images.

The accuracy of amplitude determination with ion-beam thinned specimens, however, is limited by the small area within which dynamical effects are negligible. This area is often small enough to preclude accurate electron diffraction measurements. We have used instead the information contained in the focus series of images Assuming that for each reflection the absolute value of the CTF

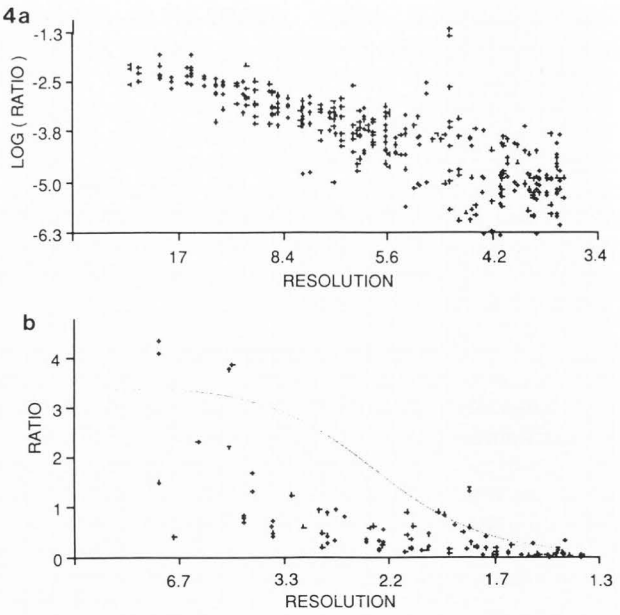

Fig. 4. Falloff of structure factor amplitudes derived from images with increasing resolution. (a) The ratio of amplitudes from one image of bR to electron diffraction amplitudes (natural log plot, image amplitudes corrected for CTF) shows a loss of image contrast by about a factor of 15 at 0.4 nm. (b) Ratio of amplitudes obtained from all staurolite images to amplitudes from calculations based on the known structure follows the form of the expected envelope function, shown as smooth curve.

would be near unity for some image in the series, we have used the highest amplitude found within the series.

The use of image amplitudes still leaves the strong effect of the envelope of the transfer function. This envelope can be accurately predicted from operating parameters, and then compensated with confidence. Figure 4b shows a plot of amplitudes obtained directly from images of staurolite relative to amplitudes predicted from the known structure. The amplitude ratio follows the form of the envelope function for the imaging parameters that were used.

It has been found that structure factor phases are much more important than amplitudes in determining the appearance of a reconstructed image. Thus we put more effort into accurate phase determination. On the other hand, compensation for the falloff of amplitudes with resolution is absolutely necessary to obtain a reconstruction that contains useful information at the highest resolution of the data. An image formed with low amplitudes for the high-resolution data will have the appearance of a lower resolution image. This effect is illustrated in Fig. 5. Figures 5a and 5b compare projections of bR at 0.35 nm resolution that would be obtained using raw image amplitudes

with the reconstruction obtained using electron diffraction amplitudes. Figures 5c and 5d are reconstructions of the 001 projection of staurolite using data to 0.14 nm and amplitudes as determined directly from the images (Fig. 5c) and after correction for the envelope function (Fig. 5d). In both cases the use of the uncorrected amplitudes gives an image that shows much less detail than is actually present in the data.

Data Merging

Once the Fourier coefficients have been extracted from the images and CTF effects corrected, data from images of the specimen in equivalent orientations can be merged to give an accurate projection, and data from all orientations can be merged to give the full 3-D density map. In the case of equivalent projections, the merging process essentially averages structure factors to improve the SNR. In order that averaging of phases makes sense, the phase origin, or position of the center of the image within a unit cell, must be the same for each image. The phase origin is chosen at the position of some symmetry axis, and appropriate phase shifts are applied to each reflection to center the image (Amos et al. 1982). Resultant phases will then obey the symmetry constraints of the structure.

Various weighting schemes have been used in combining data, all based on the SNR of individual measurements (Henderson et al. 1986; Brillinger et al. 1990). The philosophy of these schemes varies, but all weight data that appear best more heavily than lower quality data.

Merging data from images of 2-D crystals at various orientations involves assigning the positions in z^* along each lattice rod where measurements fall. The z^* position follows from the tilt angle and azimuth with respect to the lattice vectors. These parameters can be determined from the distortion of the lattice vectors that occurs upon tilting (Shaw and Hills, 1981). For 3-D crystals, the HK indices of the projections are transformed to the hkl indices of 3-D reciprocal space, and data from the various projections is sorted into a 3-D file. Once the phase origin in one projection has been set, constraining phases of reflections in other orientations that are common to the first will ensure that the same phase origin is taken for all projections.

Results

The 3-D density map of bacteriorhodopsin (Henderson et al. 1990) was synthesized from 2700 structure factors in the unique part of reciprocal space. Views of the map are shown in Fig. 6, in sections parallel to the membrane plane. It has proven more difficult to obtain high quality data

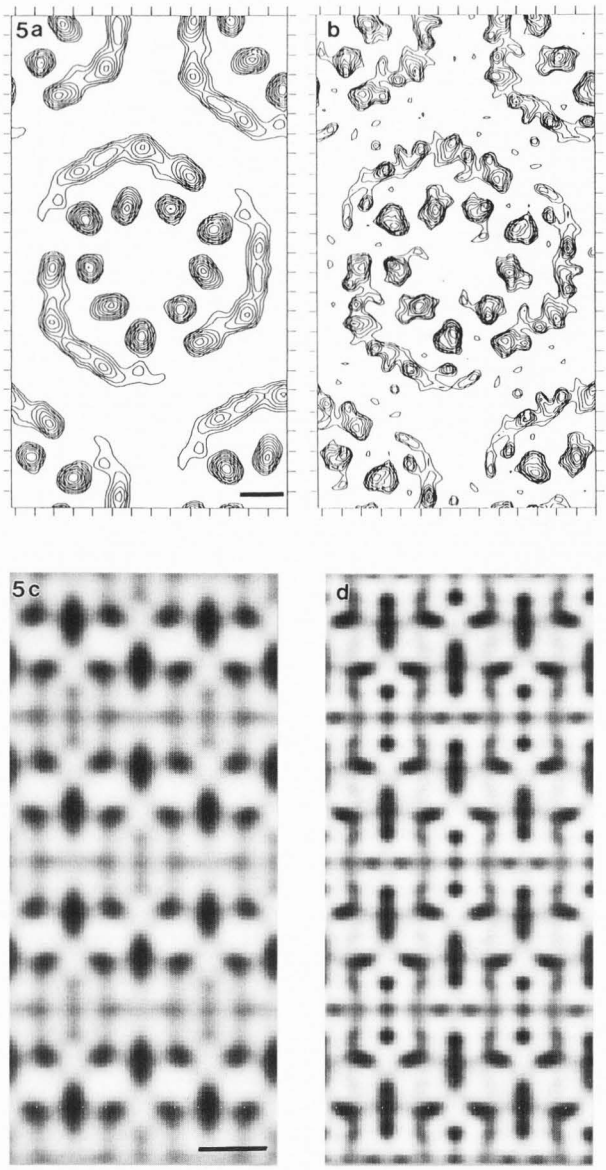

Fig. 5. Effect of correcting for amplitude falloff at high resolution. (a) Projection of bR calculated using all data to 0.35 nm (Henderson et al. 1986), but with amplitudes weighted by a factor that corresponds to the falloff observed in Fig. 4a. This image has the appearance of an image in which the resolution is actually limited to about 0.7 nm. Scale bar = 1 nm. (b) Projection of bR using electron diffraction amplitudes shows details corresponding to some of the irregular densities in the 3-D map. (c) 001 projection of staurolite calculated using data from through focus-series images. Data extends to 0.14 nm, but this image resembles images calculated with about 0.2 nm resolution. Scale bar = 0.2 nm. (d) After correcting for the CTF envelope, features close to atomic size are revealed.

from highly tilted purple membrane specimens than from untilted ones. This effect has limited the range in z^* over which accurate phase data could be collected, and thus limits the resolution of the 3-D map in the direction perpendicular to the membrane plane. Our 3-D map of bacteriorhodopsin contains data in plane to 0.35 nm, and limited data to 0.5 nm in z^*. The seven transmembrane density rods are very clearly resolved, with many bulges and bumps that can be interpreted as bulky amino acid side chains. The position of the retinal ring is also clearly resolved, in fact as the densest feature in the map.

The resolution is not nearly good enough to identify single atoms, but atom groups can be localized using the features of the map along with constraints from other studies.

The data from five orientations of staurolite (Downing et al. 1990) were merged to produce 58 independent structure factors, corresponding to 162 in half space when the symmetry operations were applied. This data samples the reciprocal lattice quite uniformly, and the resolution in the density map is quite isotropic. An iso-potential surface view of the map is shown in Fig. 7, which shows positions of the cations which are present at full occupancy. Atoms present at half occupancy have a density in this view below the contouring level. An ORTEP plot (Fig. 7b) shows atom locations calculated from X-ray data (Smith, 1968), in a similar orientation.

Details in the map are better represented in sections in Fig. 8. These sections cover one quarter of the unit cell, which is related to the rest of the structure by symmetry. Most of the atoms are located near the z=0 and z=1/4 sections, and atom positions are indicated in views of these sections, calculated from the structure determined from X-ray work.

Interpretation of the 3-D Map

We have certainly not yet reached the point where electron microscope data can produce a 3-D reconstruction in which all atoms could be identified by both type and position simply from examining the map. Resolution in protein images rarely exceeds 0.3 nm, and in bR is closer to 0.7 nm perpendicular to the membrane plane, so that only groups of atoms are resolved from each other. However, this resolution is sufficient for interpretation of the atomic structure. The reason lies in the large number of constraints on the structure. Although there can be a very large number of atoms in a single molecule (for example, nearly 2000 non-hydrogen atoms in bR), all of the atom types are known along with a wealth of information about groupings of atoms. Proteins are made up of amino acids, many of distinctive shape and with only a few variables in their conformation, which are strung together in a peptide chain of known sequence. It has been known from X-ray diffraction work that with a density map at around 0.35 nm resolution the peptide chain can be fit to the map and side chain positions readily identified (Blundell and Johnson, 1976). Refinement based on interatomic distances, energy minimization and other parameters, constrained by diffraction amplitudes at higher resolution, can then be used to improve the atomic model.

In the case of bR, most of the secondary structure was clear from the density map, with helical segments of the peptide chain running across the membrane. Even with the limited resolution of our 3-D map, it was possible to assign features of the transmembrane densities to bulky side chains. This assignment was aided and supported by extensive spectroscopic work and genetic studies which had made predictions about relative locations of many of the amino acids. The model fit to the density map was consistent with virtually all of this biophysical data, and led to further predictions about the functional mechanism of the protein.

In the case of minerals, the higher density and more compact structure requires higher resolution for identifying even atom groups. Some constraints on grouping are available from the chemistry of the sample. For example, staurolite is known as a silicate with cations in tetrahedral and octahedral coordination with oxygens. Some of these structures are identifiable in the surface representation, but the individual atoms are most clearly seen in the sections. The variations in atom density caused by partial occupancy, as well as the small depen-

Fig. 6. 3-D reconstruction of bR. (a-f) Sections spaced 0.6 nm apart, parallel to the membrane plane, are shown. In (d) the outline of the protein monomer is indicated. (g) Part of the atomic model which has been superimposed on a surface-net view of a section about 0.6 nm thick. Heavy lines represent bonds between atoms.

Fig. 7. (a) Surface representation of the 3-D reconstruction of staurolite. Densities around cation sites are well resolved, although atoms present at less than full occupancy are below the contouring density. (b) ORTEP plot in approximately the same orientation, showing all atoms, was calculated from the structure determined by X-ray diffraction (Smith, 1968).

Fig. 8. Sections through one quarter of the 3-D reconstruction of staurolite, parallel to [001], spaced 0.02 nm apart. The rest of the unit cell is related by symmetry to this quarter. Atom densities are well resolved in z=0 and z=1/4 sections, which contain the atoms as indicated below. Peak densities depend on both atom type and partial occupancy; atom types are indicated at bottom.

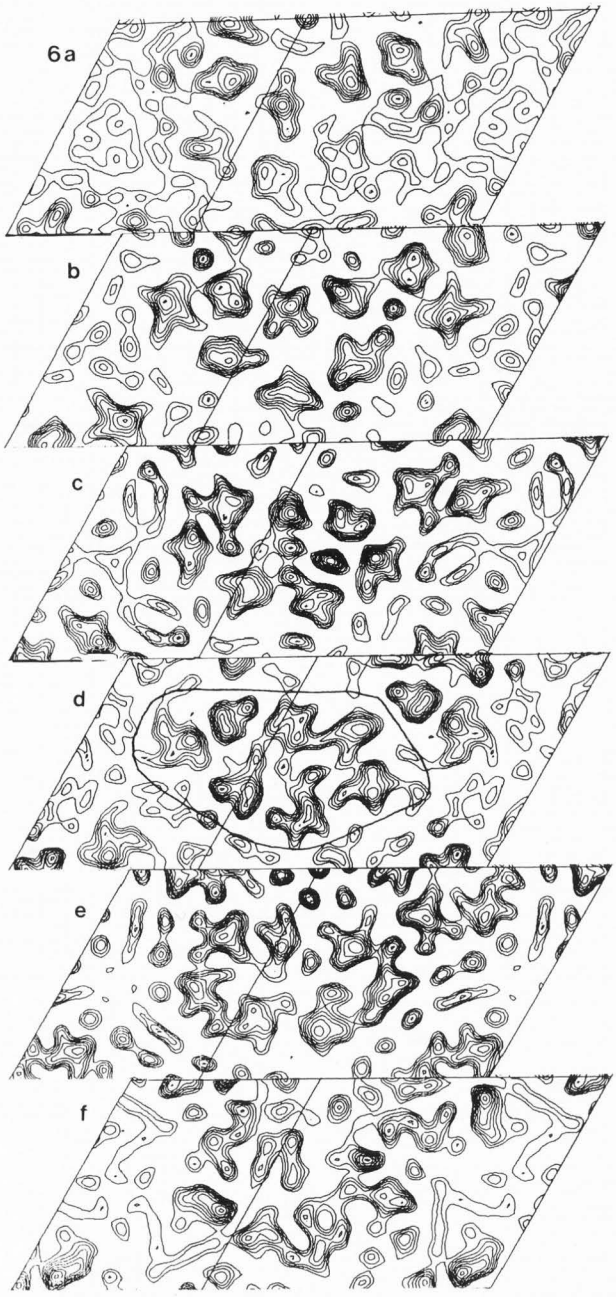

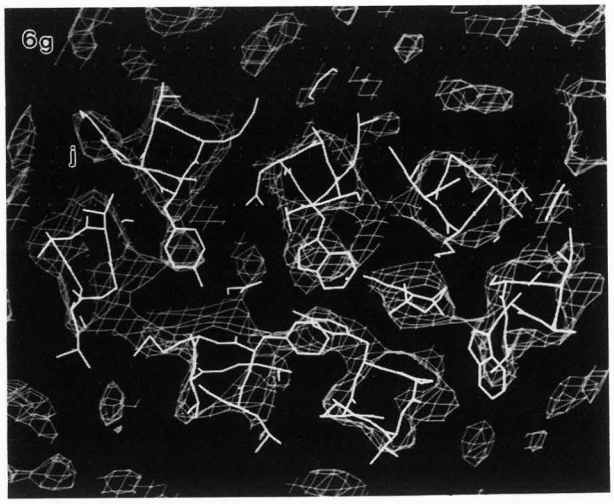

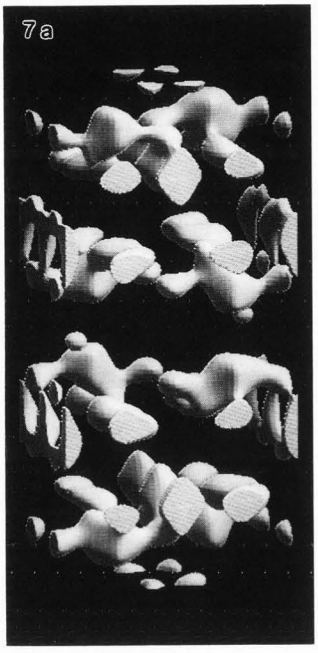

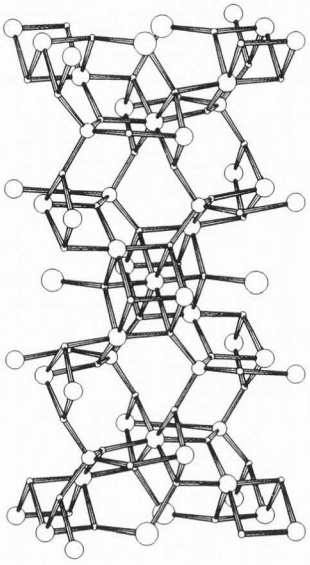

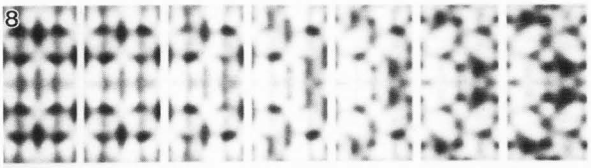

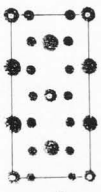

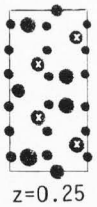

dence of electron scattering on atomic number, may make it difficult to relate peaks in the density map to particular atom types unless the chemical and other constraints are incorporated in the interpretation.

Discussion

The difference in interpretability and information content between a 2-D projection image and a 3-D reconstruction is seen by comparing the bR images in Figs. 5b and 6, and the staurolite images

of Figs. 5d and 8. Details that are entirely obscured in projection are easily seen in the 3-D reconstruction. The resolution attainable with materials samples is higher than with organic specimens for a number of reasons. Resolution in protein imaging is limited both by the inherent ordering of the samples, which rarely diffract beyond 0.2 nm, and by radiation damage, which ultimately limits the SNR in the image. Fortunately, interpretation of a 3-D density map is possible at much lower resolution in proteins than in minerals. Protein structures are characterized by relatively low density with distinctive groupings of atoms, which can be interpreted at available resolution levels, even when the resolution is quite limited in one direction. In addition, we can expect to know much about structures which are studied by electron microscopy from other biophysical and genetic studies, which help to constrain the number of possible interpretations of the map.

True atomic resolution appears necessary in order to interpret 3-D reconstructions of mineral samples. Attaining this resolution in interpretable images is limited mainly by dynamical effects with thicker crystals, but the required information can in fact be obtained from the small, very thin areas. The technique should thus be well suited to the determination of structures in which disorder limits the coherent crystal domains to a size on the order of tens of unit cells. Although it may be difficult to identify atomic species directly from the 3-D map, chemical constraints on the structure should make the interpretation unambiguous.

Acknowedgement

This work has been supported by the Office of Health and Environmental Research, U. S. Department of Energy, under contract DE-AC03-76SF000098, and by NIH grant GM26884.

References

Amos LA, Henderson R, Unwin PNT. (1982) Three-dimensional structure determination by electron microscopy of two-dimensional crystals. Prog Biophys Mol Biol 39 183-231

Baumeister W, Barth M, Hegerl R, Guckenberger R, Hahn M, Saxton WO. (1986) Three-dimensional structure of the regular surface layer (HPI layer) of *Deinococcus radiodurans*. J Mol Biol 187 241-253

Blundell TL, Johnson LN (1976) Protein crystallography. Academic Press, New York p 381 ff

Brillinger DR, Downing KH, Glaeser RM. (1990) Some statistical aspects of low-dose electron imaging of crystals. J. Stat Planning and Inference 25 235-259

Downing KH, Grano DA. (1982) Analysis of photographic emulsions for electron microscopy of two-dimensional crystalline specimens. Ultramicroscopy 7 381-404

Downing KH, Mieshing H, Wenk HR, O'Keefe MA. (1990) Resolution of oxygen with the TEM: 3D-Electron crystallography of staurolite. Nature 348 525-528

Dubochet J, Adrian M, Chang JJ, Holmo J-C, Lepault J, McDowall AW, Shultz P. (1988) Cryo-electron microscopy of vitrified biological specimens. Q Rev Biophys 21 192-228

Glaeser RM. (1985) Electron crystallography of biological macromolecules. Ann Rev Phys Chem 36 243-275

Glaeser RM, Tong L, Kim S-H. (1989) Three-dimensional reconstruction from incomplete data: Interpretability of density maps at "atomic" resolution. Ultramicroscopy 27 307-318

Henderson R, Glaeser RM. (1985) Quantitative analysis of image contrast in electron micrographs of beam-sensitive specimens. Ultramicroscopy 16 139-150

Henderson R, Baldwin JM, Downing KH, Lepault J, Zemlin F. (1986) Structure of purple membrane from *Halobacterium halobium*: recording, measurement, and evaluation of electron micrographs at 3.5 A resolution. Ultramicroscopy 16 147-178

Henderson R, Baldwin JM, Ceska T, Zemlin F, Beckmann E, Downing KH. (1990) Model for the structure of bacteriorhodopsin based on high-resolution electron cryo-microscopy. J Mol Biol 213 889-929

Hirsch PB, Howie A, Nicholson RB, Pashley DW, Whelan MJ. (1977) Electron Microscopy of Thin Crystals. Krieger, Malabar FL p 195 ff

Ho M-H, Jap BK, Glaeser RM. (1988) Validity domain of the weak-phase-object approximation in electron diffraction of thin proteins. Acta Cryst A44 878-884

O'Keefe MA, Buseck PR, Iijima S. (1978) Computed crystal structure images for high-resolution electron microscopy. Nature 274 322-324

Rose A. (1973) Vision: Human and Electronic. Plenum, New York

Shaw PJ, Hills GJ. (1981) Tilted specimens in the electron microscope: A simple specimen holder and calculation of tilt angles for crystalline specimens. Micron 12 279-282

Smith JV.(1968) The crystal structure of staurolite. Amer Mineral 53 1139-1155 p18 ff

Unwin PNT, Henderson R. (1975) Molecular structure determination by electron microscopy of unstained crystalline specimens. J Mol Biol 94 425-440

Editor's Note: All of the reviewer's concerns were appropriately addressed by text changes, hence there is no Discussion with Reviewers.